Nano Research
2022, 15(10): 9125–9134

ISSN 1998-0124 CN 11-5974/O4
https://doi.org/10.1007/s12274-022-4553-6

Research Article

Cardiomyocyte-targeted anti-inflammatory nanotherapeutics against myocardial ischemia reperfusion (IR) injury

Min Lan[1], Mengying Hou[1], Jing Yan[1] (✉), Qiurong Deng[1], Ziyin Zhao[1], Shixian Lv[1], Juanjuan Dang[1], Mengyuan Yin[1], Yong Ji[2] (✉), and Lichen Yin[1] (✉)

[1] *Institute of Functional Nano and Soft Materials (FUNSOM), Jiangsu Key Laboratory for Carbon-Based Functional Materials and Devices, Soochow University, Suzhou 215123, China*

[2] *Department of Cardiothoracic Surgery, Wuxi People's Hospital Affiliated to Nanjing Medical University, Wuxi 214023, China*

Received: 7 April 2022 / **Revised:** 11 May 2022 / **Accepted:** 16 May 2022

ABSTRACT

Myocardial ischemia reperfusion (IR) injury is closely related to the overwhelming inflammation in the myocardium. Herein, cardiomyocyte-targeted nanotherapeutics were developed for the reactive oxygen species (ROS)-ultrasensitive co-delivery of dexamethasone (Dex) and RAGE small interfering RNA (siRAGE) to attenuate myocardial inflammation. PPTP, a ROS-degradable polycation based on PGE_2-modified, PEGylated, ditellurium-crosslinked polyethylenimine (PEI) was developed to surface-decorate the Dex-encapsulated mesoporous silica nanoparticles (MSNs), which simultaneously condensed siRAGE and gated the MSNs to prevent the Dex pre-leakage. Upon intravenous injection to IR-injured rats, the nanotherapeutics could be efficiently transported into the inflamed cardiomyocytes via PGE_2-assisted recognition of over-expressed E-series of prostaglandin (EP) receptors on the cell membranes. Intracellularly, the over-produced ROS degraded PPTP into small segments, promoting the release of siRAGE and Dex to mediate effective RAGE silencing (72%) and cooperative anti-inflammatory effect. As a consequence, the nanotherapeutics notably suppressed the myocardial fibrosis and apoptosis, ultimately recovering the systolic function. Therefore, the current nanotherapeutics represent an effective example for the co-delivery and on-demand release of nucleic acid and chemodrug payloads, and might find promising utilities toward the synergistic management of myocardial inflammation.

KEYWORDS

small interfering RNA (siRNA) delivery, reactive oxygen species (ROS) responsiveness, ditellurium-crosslinked polyethylenimine (PEI), myocardial ischemia reperfusion injury, anti-inflammation

1 Introduction

Myocardial infarction accounts for more than 7 million deaths annually [1–4]. Reperfusion represents a major approach to rescue the ischemic myocardium. Nevertheless, blood reperfusion at the meantime will cause free radical burdens via excessive production and accumulation of reactive oxygen species (ROS), thereby causing the cascaded inflammatory reactions in the myocardium [5, 6]. Consequently, myocardial ischemia reperfusion (IR) injury is induced, which provokes cardiomyocyte death and scar tissue formation to impair the cardiac function [7–9]. As such, anti-inflammatory treatment represents an important paradigm against myocardial IR injury.

RNA interference (RNAi), often mediated by small interfering RNA (siRNA), represents a robust mechanism to silence the abnormally up-regulated gene expression by degrading the mRNA in a sequence-defined manner [10–13]. The unique advantages of RNAi, including high efficiency, sequence specificity, and fewer side effects, have made it a promising modality for anti-inflammation treatment by silencing the expression of inflammation-related genes [14–17]. Among them, the pattern-recognition receptor for advanced glycation end product (RAGE) is an important mediator that regulates the pro-inflammatory and pro-apoptotic processes in the IR-injured myocardium by accumulating various ligands at the inflammation area [18–20]. Therefore, siRNA-mediated RNAi against RAGE in cardiomyocytes holds great potentials as a therapeutic paradigm for myocardial IR injury.

To fulfill high-efficiency gene silencing *in vivo*, an appropriate siRNA delivery vehicle is highly demanded to overcome the various systemic and cellular barriers, such as the hydrolytic degradation of siRNA by nucleases, insufficient targeting to and accumulation at the diseased tissues, inefficient transport across cell membranes, and endolysosomal degradation of gene cargoes [21–27]. Cationic polymers, also termed as polycations, are widely adopted materials for siRNA delivery, mainly because they can form nanocomplexes (NCs) with siRNA upon electrostatic assembly and thereby facilitate the trans-membrane delivery into the cytosol [28–30]. However, polycations often face a critical dilemma related to siRNA condensation and release. Normally, polycations with higher molecular weights (MWs) feature stronger siRNA condensation and intracellular delivery efficiencies. However, they will impede the cytosolic release of siRNA to compromise the transfection efficiency and induce MW-

Address correspondence to Jing Yan, jyan@suda.edu.cn; Yong Ji, jiyongmyp@163.com; Lichen Yin, lcyin@suda.edu.cn

dependent long-term toxicity [31–33]. To address this dilemma, ROS-degradable polycations have been developed and utilized for delivering siRNA into inflamed cells that produce elevated levels of ROS [34–37]. However, the disease-relevant ROS level (50–200 μM) is often insufficient for majority of the reported ROS-responsive materials [38]. For instance, diselenide-containing polymers can only be degraded at the H_2O_2 concentration of 1–5 mM. Because Te has weaker electronegativity than Se and Te–Te also has much lower bond energy (126 kJ/mol) than Se–Se (172 kJ/mol), ditellurium-containing polymers should have higher sensitivity to ROS [39–41]. Besides the dilemma associated with siRNA encapsulation and release, the polycation/siRNA NCs with positive surface charges are instable during blood circulation, because the negatively charged serum proteins will adsorb onto the NCs surface and ultimately cause the NCs clearance by reticuloendothelial tissues [42–45]. As such, it is highly imperative to develop serum-stable, cardiomyocyte-targeted NCs that can intracellularly liberate the siRNA cargo in response to the endogenous ROS level inside inflamed cardiomyocytes.

Because the inflammation reaction is associated with complex cellular pathways and genetic mechanisms, single-target treatment is often suboptimal [46]. Combination therapy using multiple drugs can largely overcome this issue, because it can manipulate multiple targets or pathways [47–49]. Particularly, combination of siRNA with a small-molecular chemodrug may enable synergistic anti-inflammatory effect [50]. Dexamethasone (Dex), a glucocorticoid drug in the clinic that can suppress inflammation by inhibiting the NF-κB pathway, could thus be co-delivered with RAGE siRNA (siRAGE) to reinforce the anti-inflammatory efficacy [51, 52].

With the attempt to achieve efficient and cardiomyocyte-targeted co-delivery of siRAGE and Dex, NCs based on mesoporous silica nanoparticles (MSNs) coated with the ROS-ultrasensitive polycation were herein developed. MSNs were adopted to load Dex inside the cavity, and were thereafter enveloped with PGE_2-PEG modified tellurium-crosslinked polyethyleneimine (PPTP), ditellurium-crosslinked polyethylenimine (PEI) conjugated with prostaglandin E_2-modified poly(ethylene glycol) (PGE_2-PEG). PPTP not only served as the gating material of MSNs to prevent non-specific Dex leakage, but also loaded siRAGE via electrostatic complexation. Upon systemic administration, the NCs could target and enter cardiomyocytes due to the binding affinity of PGE_2 to the over-expressed E-series of prostaglandin (EP) receptors on cardiomyocyte surfaces. In the inflamed cardiomyocytes, PPTP degraded into low-MW segments in response to the over-produced ROS (0.1 mM), facilitating the intracellular siRAGE release and thereby enhancing the RAGE silencing efficiency. Meanwhile, PPTP-mediated gating was weakened, which simultaneously promoted Dex release from the MSNs. Finally, Dex and siRAGE cooperated to attenuate the myocardial inflammation and recover the cardiac function after myocardial IR injury (Scheme 1).

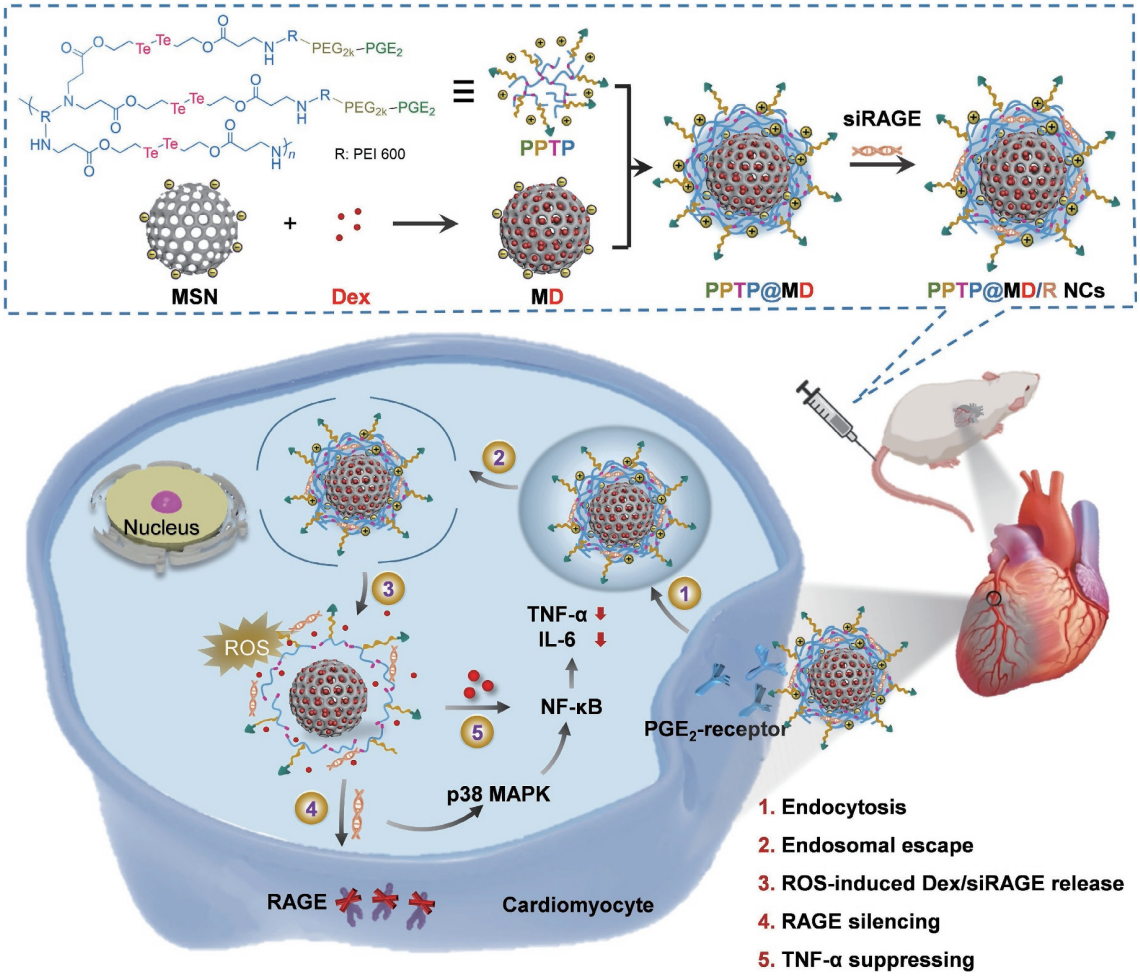

Scheme 1 Cardiomyocyte-targeted anti-inflammatory nanotherapeutics for the ROS-ultrasensitive co-delivery of siRAGE and Dex. Dex-loaded MSNs were enveloped with PPTP, the ditellurium-containing polycation, which further complexed with siRAGE and simultaneously gated MSNs to prevent pre-leakage of Dex. After systemic injection to myocardial IR-injured rats, the nanotherapeutics could be efficiently transported into the inflamed cardiomyocytes via PGE_2-assisted recognition of over-expressed EP receptors on the cell membranes. Thereafter, PPTP was sensitively degraded into low-MW segments by the intracellular ROS, releasing the siRAGE and Dex to provoke efficient RAGE silencing and cooperative management of myocardial inflammation.

2 Results and discussion

2.1 Synthesis and characterization of PPTP and MSNs

PEI 600 was crosslinked with ditellurium-containing **compound 2** through the Michael addition reaction, and the obtained tellurium-crosslinked polyethyleneimine (TP) was further conjugated with PGE_2-PEG_{2k}-COOH through the amidation reaction to ultimately yield PPTP (Scheme S1 in the Electronic Supplementary Material (ESM)) [53]. The chemical structures of **compound 2** (crosslinker) and PPTP were verified by ^1H nuclear magnetic resonance (NMR) (Figs. S1–S3 in the ESM). PGE_2-PEG modified carbon-crosslinked polyethyleneimine (PPCP), a non-responsive counterpart of PPTP, was similarly prepared by crosslinking PEI 600 with HGDA instead of **compound 2** followed by conjugation with PGE_2-PEG_{2k}-COOH (Scheme S1 in the ESM). Gel permeation chromatography (GPC) analysis further characterized the MWs and ROS-responsiveness of PPTP and PPCP (Table S3 in the ESM), wherein PPTP but not PPCP was efficiently degraded by H_2O_2 treatment (0.1 mM, 12 h).

MSNs were synthesized via the one-pot method [54, 55] and Fourier transform infrared spectroscopy (FTIR) spectrum confirmed the successful synthesis of MSNs (Fig. S4 in the ESM). Brunauer–Emmett–Teller (BET) and Barrett–Joyner–Halenda (BJH) analyses [56] revealed the surface area (1,393 m^2/g) and the pore size (2.4 nm) of the MSNs (Figs. S5 and S6 in the ESM). The MSNs adopted spherical shape with the mean diameter of ~ 130 nm as shown in the transmission electron microscopy (TEM) image, and an ordered mesoporous network was observed at higher magnification (Fig. S7 in the ESM).

2.2 Preparation and characterization of NCs

The negatively charged MSNs were coated with the positively charged PPTP to prepare the PPTP@M NCs. When the PPTP/MSNs weight ratio was increased from 1:40 to 1:1, the zeta potential of NCs increased, reaching ~ 20 mV at the PPTP/MSNs weight ratio of 1:10 (Fig. S8 in the ESM). Further increment of the PPTP/MSNs ratio did not significantly enhance the positive zeta potential. Therefore, the optimal PPTP/MSNs weight ratio of 1:10 was identified and used for all the following studies. TEM result revealed that PPTP@M NCs also possessed spherical morphology with a thin layer of polymeric shell (Fig. S9 in the ESM).

PPTP@M NCs (PPTP/MSNs = 1:10, w/w) were allowed to complex with siRAGE via electrostatic interaction, forming the PPTP@M/R NCs. Agarose gel electrophoresis image depicted that PPTP@M NCs could effectively condense siRAGE at the PPTP/siRAGE weight ratio ≥ 5 (Fig. S10(a) in the ESM). When the PPTP/siRAGE weight ratio reached 6, positively charged PPTP@M/R NCs (zeta potential of ~ 18 mV) were obtained, which adopted the hydrodynamic size of ~ 200 nm (Fig. S10(b) in the ESM). As the PPTP/siRAGE weight ratio was further increased, neither the zeta potential nor the particle size was appreciably changed. As thus, the optimal PPTP/siRNA weight ratio of 6 was identified and used for all the following studies. NCs encapsulating scrambled siRNA (siScr) were similarly prepared, and the abbreviations of all tested NCs in this study were listed in Table S4 in the ESM.

To prepare the Dex-loaded NCs, Dex was first encapsulated into the hollow cavity of MSNs via hydrophobic interaction, followed by surface decoration with PPTP and complexation with siRAGE. The drug loading efficiencies (DLE) and drug loading content (DLC) of Dex in the PPTP@MD NCs at the Dex/(PPTP@M) weight ratio of 0.5 were 16.9% and 7.8%, respectively, as determined by high performance liquid chromatography (HPLC) (Fig. S11 in the ESM). Further increase of the Dex/(PPTP@M) weight ratio to 1 led to notably decreased DLE and slightly increased DLC. Therefore, the optimal Dex/(PPTP@M) weight ratio of 0.5 and PPTP/siRAGE weight ratio of 6 were identified to prepare the final PPTP@MD/R NCs. PPTP@MD/R NCs possessed comparable zeta potential and hydrodynamic size to the Dex-unloaded NCs (~ 16 mV and ~ 216 nm for PPTP@MD/R NCs; ~ 18 mV and ~ 200 nm for PPTP@M/R NCs), indicating that the encapsulated Dex had unappreciable influence on the physicochemical properties of NCs (Fig. S12 in the ESM). The gel electrophoresis assay further verified that the siRNA condensation by PPTP was not influenced by Dex encapsulation into the NCs (Fig. S13 in the ESM). In similar, the non-responsive PPCP@MD NCs could also effectively condense siRAGE at the PPCP/siRAGE weight ratio ≥ 6 (Fig. S14 in the ESM).

We then explored the serum stability of NCs, an important feature that systemically delivered NCs should possess. As depicted in Fig. 1(a), particle size of TP@MD/R NCs markedly increased from 200 to 480 nm after 4 h incubation in serum, which mainly ascribed to the adsorption of negatively charged serum proteins onto the surface of the polycationic NCs. In contrast, size of the PPTP@MD/R NCs remained almost unchanged within 4 h, because the hydrophilic PEG chains in PPTP could repel the binding of serum proteins. Then, the capability of NCs to prevent siRNA from enzymatic degradation by serum nucleases was further probed. As revealed by the electrophoresis image (Fig. 1(b)), naked siRAGE was remarkably degraded after serum treatment for 6 h, while encapsulated siRAGE in the PPTP@MD/R NCs maintained stable, as evidenced by the unappreciably changed band intensity after serum treatment. Such property of the NCs was mainly attributed to the effective condensation of siRNA by PPTP that prevented the approaching of nucleases.

2.3 ROS-responsive siRNA/Dex release

We then probed the ROS-responsive siRNA release from NCs. After PPTP@MD/R NCs were incubated with 0.1 mM H_2O_2 for up to 12 h, siRAGE migration was detected at the PPTP/siRAGE weight ratios of 6 and 8 after electrophoresis, and longer incubation time correlated to more pronounced siRAGE migration (Fig. 1(c)). Moreover, the size of PPTP@MD/R NCs (220 nm) was elevated to 425 nm upon H_2O_2 treatment (0.1 mM, 12 h, Fig. 1(d)). It therefore implied the disassembly of NCs and siRNA release in response to ROS. As the non-responsive control, siRAGE condensation by PPCP@MD/R NCs was not obviously affected after H_2O_2 treatment (0.1 mM) for 12 h (Fig. S15 in the ESM). Consistently, particle size of the PPCP@MD/R NCs was not changed after the same H_2O_2 treatment (Fig. 1(d)). Such discrepancy between PPTP@MD/R NCs and PPCP@MD/R NCs substantiated that PPTP could be efficiently degraded at the endogenous ROS concentration inside inflamed cardiomyocytes to facilitate siRNA unpackaging.

Afterwards, the ROS-responsive Dex release from NCs was also monitored in PBS (pH 7.4) or PBS (pH 7.4) supplemented with 0.1 mM H_2O_2. As shown in Fig. S16 in the ESM, ~ 80% of the encapsulated Dex could be quickly released from MD at pH 7.4 within 6 h, mainly due to their porous structure. However, Dex release from PPTP@MD/R NCs and PPCP@MD/R NCs was dramatically retarded, which could be attributed to the polymeric envelope on the surface of MSNs that gated to prevent the Dex leakage (Fig. 1(e)). In comparison, in the presence of H_2O_2 (0.1 mM), Dex release from the ROS-responsive PPTP@MD/R NCs but not the non-responsive PPCP@MD/R NCs was notably enhanced, and within 12 h, more than 75% of the loaded Dex was liberated from the NCs. The above results thus indicated that the

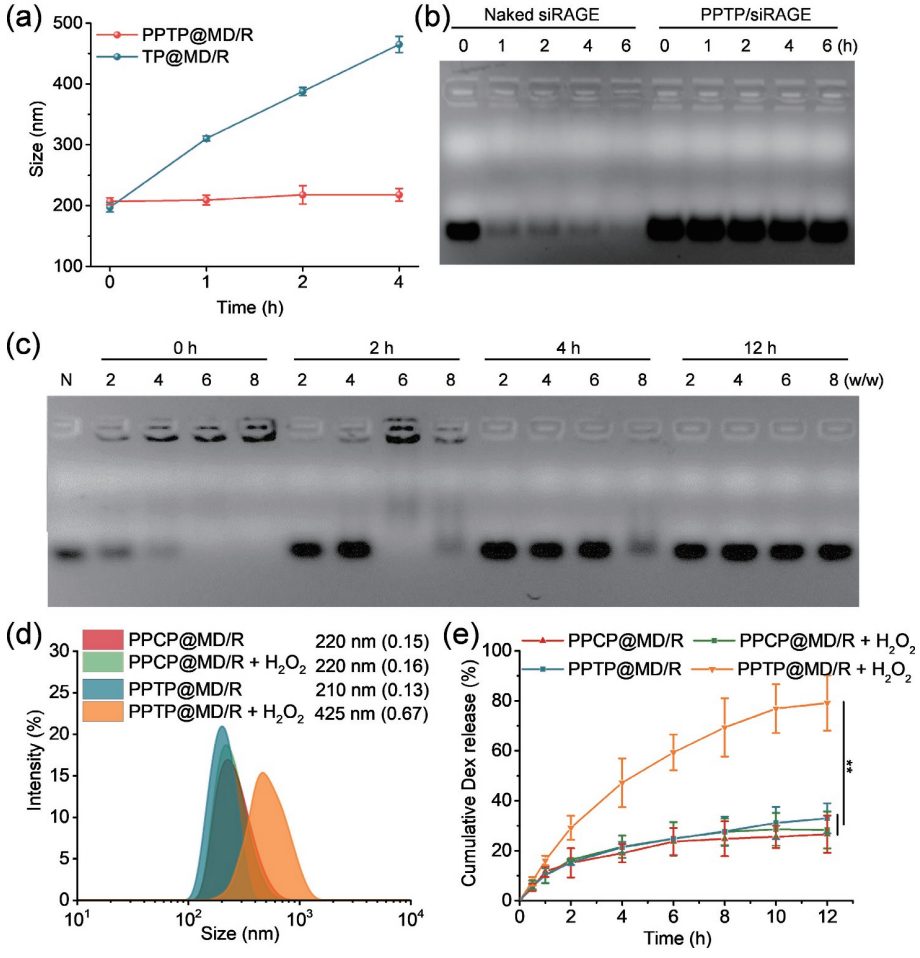

Figure 1 Characterization of NCs and ROS-responsive cargo release. (a) Time-dependent size change of TP@MD/R NCs and PPTP@MD/R NCs in FBS (10%)-containing Dulbecco's modified eagle medium (DMEM) (n = 3). (b) Stability of naked siRAGE and siRAGE encapsulated in PPTP@MD/R NCs following treatment with rat serum for different time. N represents naked siRAGE without serum treatment. (c) siRAGE release from PPTP@MD/R NCs (PPTP/siRAGE weight ratios of 2, 4, 6, and 8) following H_2O_2 (0.1 mM) treatment for different time. N denotes naked siRAGE. (d) Size distribution of PPTP@MD/R NCs and PPCP@MD/R NCs with or without 12 h H_2O_2 treatment (0.1 mM). The values in the parentheses denote the polydispersity index of NCs. (e) *In vitro* Dex release from PPTP@MD/R NCs and PPCP@MD/R NCs in PBS (pH 7.4) or PBS (pH 7.4) supplemented with 0.1 mM H_2O_2 (n = 3). Differences were assessed to be significant at $^*p < 0.05$ and very significant at $^{**}p < 0.01$ and $^{***}p < 0.001$.

ROS-triggered degradation of PPTP could simultaneously promote the release of Dex and siRAGE.

2.4 Cardiomyocyte internalization and intracellular distribution of NCs *in vitro*

The gene silencing efficiency of siRNA-containing NCs heavily depends on their cellular internalization efficiency and the intracellular fate. Thus, we first determined the cytosolic delivery efficiency of NCs containing FAM-siScr in H9C2 cells. Flow cytometric and spectrofluorimetric analyses revealed that PPTP@MD/S NCs greatly enhanced the cellular internalization level of FAM-siScr (Figs. 2(a) and 2(b), and Fig. S17 in the ESM) after 4-h incubation, significantly outperforming the non-targeted PTP@MD/S NCs and commercial polycationic transfection reagent PEI 25k. It therefore indicated that PGE_2, the targeting ligand in PPTP, could help enhance the internalization level of NCs because it can bind the over-expressed EP receptors on the cardiomyocyte surfaces. Additionally, confocal laser scanning microscopy (CLSM) observation on H9C2 cells revealed that after 4-h incubation with FAM-siScr-containing NCs, the internalized FAM-siScr (green fluorescence) largely separate from Lysotracker red-stained endolysosomes (red fluorescence), verifying that the NCs could effectively escape from the entrapment by endolysosomes (Fig. 2(c)).

We further explored the cytosolic siRNA liberation from NCs via CLSM observation of hypoxia-challenged H9C2 cells that were incubated with RhB-PPTP- and FAM-siScr-containing NCs for 4 h (Fig. 2(d)). In hypoxia-challenged H9C2 cells with over-produced ROS, it was clearly noted that the green fluorescence (FAM-siScr) was separated from the red fluorescence (RhB-PPTP), and the colocalization ratio was calculated to be ~ 32%. Comparatively, greatly higher colocalization ratios were noted for PPCP@MD/S NCs under hypoxia (~ 79%) or PPTP@MD/S NCs under normoxia (~ 77%). Such disparity therefore substantiated that PPTP could be efficiently degraded by the over-produced ROS in inflamed cardiomyocytes, facilitating the intracellular siRNA release.

2.5 RAGE/TNF-α knockdown efficiencies of NCs in H9C2 cells

The capability of NCs to silence RAGE expression was first explored in hypoxia-treated H9C2 cells. As shown in Fig. 2(e), PPTP@M/R NCs remarkably down-regulated the RAGE mRNA level by ~ 71%, significantly outperforming the non-targeted PTP@M/R NCs (~ 54%). It thus indicated that the NCs could mediate effective RAGE down-regulation due to siRAGE-mediated sequence-specific mRNA degradation, wherein modification of the PGE_2 targeting ligand reinforced the efficiency of NCs due to the enhanced internalization by cardiomyocytes. PPTP@MD/R NCs showed comparable RAGE silencing efficiency

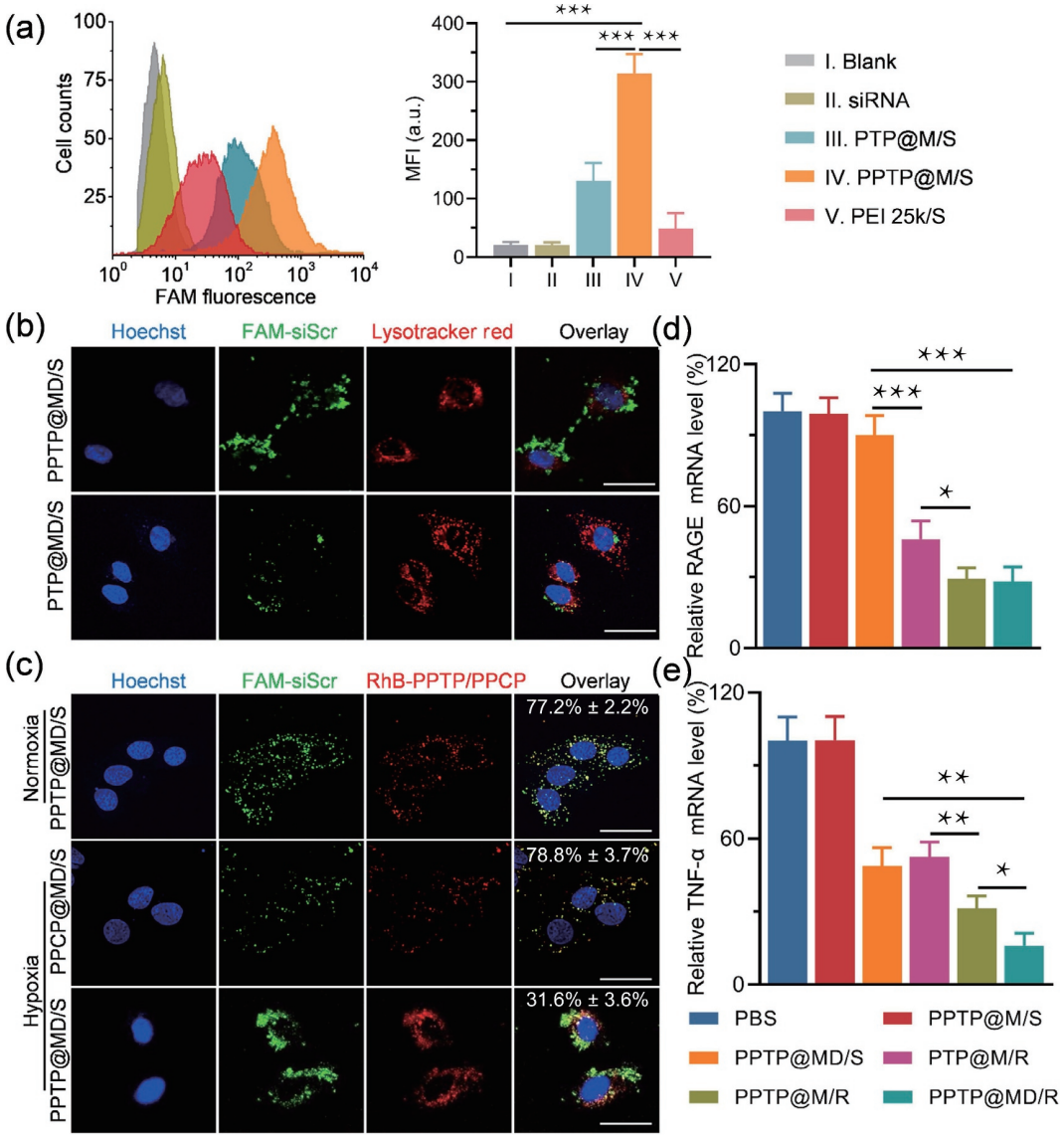

Figure 2 NCs-mediated cytosolic delivery and RAGE silencing efficiencies in H9C2 cells. (a) Flow cytometric diagrams and mean fluorescence intensity (MFI) of hypoxia-challenged H9C2 cells following incubation with naked FAM-siScr or FAM-siScr-encapsulated NCs (1 μg FAM-siScr/mL) for 4 h (n = 3). (b) CLSM images of hypoxia-challenged H9C2 cells following incubation with FAM-siScr-encapsulated PTP@MD/S NCs and PPTP@MD/S NCs for 4 h (scale bar = 50 μm). Endolysosomes and nuclei were stained with Lysotracker red and Hoechst 33258, respectively. (c) CLSM images of H9C2 cells following 4-h treatment with NCs comprised of RhB-PPTP and FAM-siScr under either hypoxic or normoxic condition (scale bar = 50 μm). The colocalization ratios between FAM-siScr and RhB-PPTP were listed (n = 20). Relative mRNA levels of RAGE (d) and TNF-α (e) in hypoxia-challenged H9C2 cells following NCs treatment (5.1 μg Dex/mL, 1 μg siRNA/mL, n = 3). Differences were assessed to be significant at $^{*}p < 0.05$ and very significant at $^{**}p < 0.01$ and $^{***}p < 0.001$.

to PPTP@M/R NCs, while PPTP@MD/S NCs and PPTP@M/S NCs showed negligible RAGE silencing efficiency, suggesting that the encapsulated Dex did not affect the RAGE silencing efficiency of NCs.

The TNF-α mRNA level in H9C2 cells was then monitored. In consistence with the RAGE silencing efficiency, PPTP@M/R NCs significantly outperformed the PTP@M/R NCs in down-regulating TNF-α (Fig. 2(e)). More noteworthy, PPTP@MD/R NCs provoked significantly higher TNF-α silencing efficiency (~ 84%) than PPTP@MD/S NCs (~ 52%, Dex only) and PPTP@M/R NCs (~ 69%, siRAGE only), which demonstrated the collaborative effect of Dex and siRAGE in inhibiting TNF-α, a critical pro-inflammatory cytokine during the inflammation cascade.

2.6 Cytotoxicity of NCs in H9C2 cells

As determined by the 3-[4,5-dimethylthiazol-2-yl]-2,5-diphenyltetrazolium bromide (MTT) assay, PPTP@M/R NCs pre-treated with H_2O_2 displayed lower cytotoxicity in H9C2 cells than those without H_2O_2 pre-treatment (Fig. S18 in the ESM), mainly because PPTP could be degraded into small species by ROS to diminish the MW-dependent material toxicity. In support of such finding, H_2O_2 pre-treatment did not diminish the cytotoxicity of PPCP@M/R NCs that were non-responsive to ROS. It thus suggested that PPTP was able to degrade in response to over-produced ROS in inflamed cardiomyocytes, thereby diminishing the polycation-induced cytotoxicity. At the PPTP concentration used for the transfection study (6 μg/mL), the NCs caused unappreciable cytotoxicity, which ensured their safe utility.

2.7 *In vivo* RAGE/TNF-α suppression in myocardium after myocardial IR injury

Before the exploration of the *in vivo* anti-inflammatory efficacy of NCs against myocardial IR injury, the targeted delivery of NCs into cardiomyocytes was first evaluated by using flow cytometry. As shown in Fig. 3(a), only ~ 15% cardiomyocytes internalized the FAM-siScr-containing PTP@M/S NCs after i.v. injection. Comparatively, nearly 50% of the cardiomyocytes had taken up

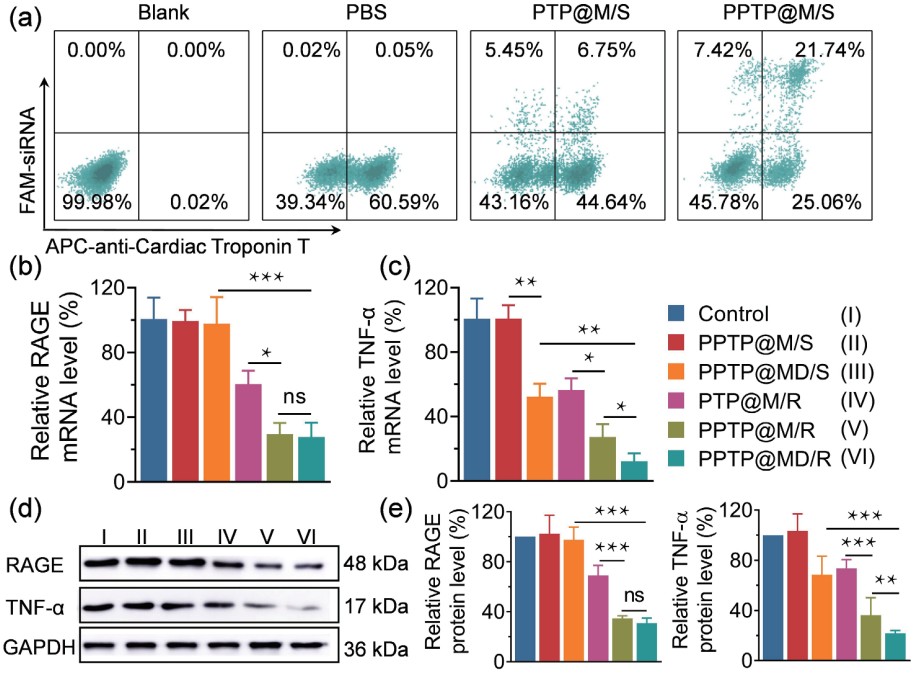

Figure 3 NCs-mediated cardiomyocyte targeting, myocardial RAGE silencing, and anti-inflammation after systemic administration in rats experiencing myocardial IR injury. (a) Flow cytometric diagrams of rat cardiomyocytes at 4 h post i.v. injection of PBS or FAM-siScr-encapsulated NCs (300 μg siRNA/kg). Cardiomyocytes were labeled with APC-anti-Cardiac Troponin T. Cells without labeling served as the blank. Relative mRNA levels of RAGE (b) and TNF-α (c) in the IR-injured myocardium (n = 4). (d) Protein levels of RAGE and TNF-α in the IR-injured myocardium as resolved by Western blot. (e) Quantification of the relative protein levels of RAGE and TNF-α from Western blot in (d) (n = 4). At 10 min post myocardial IR injury, NCs were i.v. injected at 1.54 mg Dex/kg and 300 μg siRNA/kg, and analyses in (b)–(e) were performed at 24 h post injection. Differences were assessed to be significant at $^{*}p < 0.05$ and very significant at $^{**}p < 0.01$ and $^{***}p < 0.001$.

the PPTP@M/S NCs. It again demonstrated that the systemically administered PPTP@M/S NCs could target the cardiomyocytes due to the binding affinity between the targeting ligand PGE_2 and over-expressed EP receptors on the cell surfaces.

As a consequence of the effective delivery into cardiomyocytes, PPTP@M/R NCs and PPTP@MD/R NCs provoked notable down-regulation of RAGE mRNA level by ~ 70% and ~ 72% in the ischemic myocardium, respectively, outperforming the non-targeted PTP@M/R NCs (~ 40%, Fig. 3(b)). In similar to the *in vitro* findings, PPTP@MD/R NCs featured significantly higher TNF-α mRNA silencing efficiency (~ 88%) than PPTP@M/R NCs (~ 73%) and PPTP@MD/S NCs (~ 48%), again substantiating the cooperative effect between Dex and siRAGE in attenuating cardiac inflammation post IR injury (Fig. 3(c)). Similar results were noted in terms of the myocardial levels of RAGE and TNF-α proteins as analyzed by Western blot (Figs. 3(d) and 3(e)). Collectively, these findings again demonstrated that the PPTP@MD/R NCs could efficiently target and enter inflamed cardiomyocytes after systemic administration, and thereafter release the siRAGE and Dex in consequence to the ROS-responsive degradation of PPTP, ultimately imparting cooperative effect to inhibit myocardial inflammation and protect animals from myocardial IR injury.

2.8 NCs-mediated reduction of myocardial infarction, cardiomyocyte apoptosis, and cardiac fibrosis

2,3,5-Triphenyl-2H-tetrazolium chloride (TTC) staining was used to investigate the myocardial infarction (Figs. 4(a) and 4(b)), wherein the infarcted area remained unstained (white) while the normal area was stained to appear red color [19]. Consistent with their anti-inflammatory capabilities, PPTP@MD/R NCs remarkably reduced the infarcted area, and the calculated infarct size on day 3 post NCs administration was represented by the order of PPTP@MD/R NCs (~ 10%) < PPTP@M/R NCs (~ 16%) < PTP@M/R NCs (~ 24%) < PPTP@MD/S NCs (~ 23%) < PPTP@M/S NCs (~ 46%) ≈ PBS (~ 44%).

Myocardial IR will cause tissue injury, cardiomyocyte apoptosis, and myocardial fibrosis [19]. Therefore, the myocardium injury was investigated via hematoxylin & eosin (H&E) staining; cardiac fibrosis was characterized by Masson's trichrome (MT)-stained collagen deposition; cardiomyocyte apoptosis was evaluated using the TdT-mediated dUTP nick end labeling (TUNEL) assay. The normal cardiac tissues displayed thin and compact arrangements of cardiac cells in H&E staining images, whereas rat hearts with IR injury showed atrophy and proliferation of fiber-connective tissues (Fig. 4(c)). Comparatively, such abnormality was greatly attenuated by PPTP@MD/R NCs, as evidenced by the compact arrangement of cardiac cells. Massive collagen deposition (stained in blue) was detected in rat hearts with IR injury, while it was dramatically alleviated upon PPTP@MD/R NCs treatment. The apoptosis of cardiomyocytes following IR injury was dramatically reduced by PPTP@MD/R NCs, and represented in the order of PPTP@MD/R NCs (~ 13%) < PPTP@M/R NCs (~ 31%) < PTP@M/R NCs (~ 51%) < PPTP@MD/S NCs (~ 59%) < PPTP@M/S NCs (~ 79%) ≈ PBS (~ 79%) (Fig. 4(d)). In consistence, the calculated fibrosis area was represented in the following order of PPTP@MD/R NCs (~ 7%) < PPTP@M/R NCs (~ 20%) < PTP@M/R NCs (~ 31%) ≈ PPTP@MD/S NCs (~ 30%) < PPTP@M/S NCs (~ 42%) ≈ PBS (~ 41%) (Fig. 4(e)). In together, these results verified the high efficiency of the systemically injected, cardiomyocyte-targeted PPTP@MD/R NCs in attenuating infarction size and inhibiting muscle degeneration, cardiomyocyte apoptosis, and myocardial fibrosis, which were closely related to the cooperation of siRAGE and Dex in inhibiting the overwhelming inflammation post myocardial IR injury.

2.9 NCs-mediated recovery of cardiac function

Finally, the recovery of cardiac function was monitored by M-mode echocardiography on day 3 post myocardial IR injury. Particularly, ejection fraction (EF) and fraction shortening (FS), two important indicators of the systolic function of the left ventricle, were determined. As shown in Fig. 5(a), expansion of

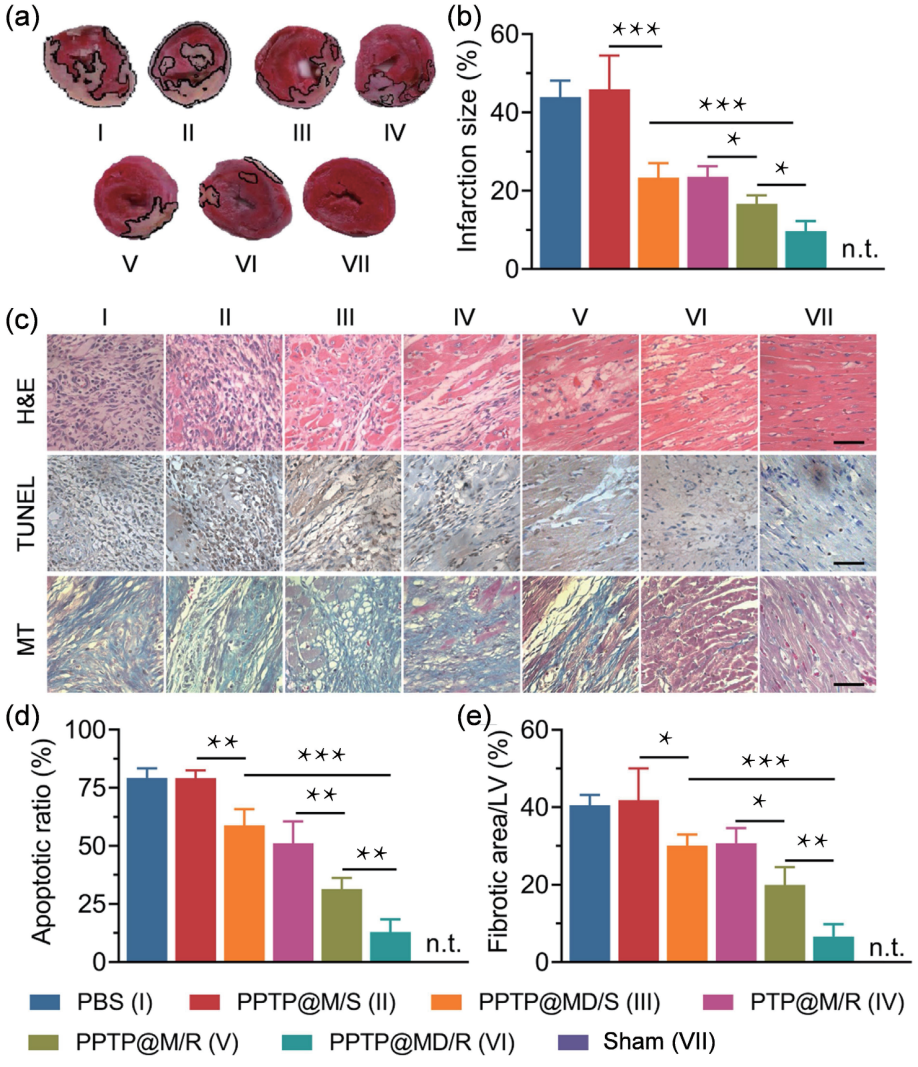

Figure 4 NCs-mediated decrease of myocardial infarct size, inhibition of cardiomyocyte apoptosis, and attenuation of myocardium fibrosis in IR-injured rats after i.v. injection. (a) Photographs of TTC-stained, IR-injured myocardium sections. (b) Infarct size of the left ventricular myocardium (n = 4). (c) Optical images of H&E-, TUNEL-, or MT-stained, IR-injured myocardium sections (scale bar = 50 μm). Calculated cardiomyocyte apoptosis ratio (d) and myocardium fibrotic area (e) from TUNEL and MT staining images, respectively (n = 4). At 10 min post myocardial IR injury, PBS or NCs were i.v. injected at 1.54 mg Dex/kg and 300 μg siRNA/kg, and all the above analyses were performed at 7 days post injection. Healthy rats without myocardial IR injury were incorporated as the normal control. Differences were assessed to be significant at $^{*}p < 0.05$ and very significant at $^{**}p < 0.01$ and $^{***}p < 0.001$.

chamber dimensions was noted for rat hearts after IR injury, which nevertheless, was dramatically alleviated after treatment with PPTP@MD/R NCs. Moreover, the ventricular wall motion of rats treated with PPTP@MD/R NCs was similar to that of sham rats. In consistence, after treatment with PPTP@MD/R NCs, EF and FS values of rat hearts almost recovered to the normal levels, significantly higher than those observed for rat hearts treated with other tested NCs (Figs. 5(b) and 5(c)). These results therefore substantiated that systemically administered PPTP@MD/R NCs could effectively reduce cardiac remodeling and propel the restoration of cardiac functions after IR injury by provoking potent anti-inflammatory outcomes.

2.10 Biocompatibility of NCs

The biocompatibility of PPTP@MD/R NCs was evaluated after i.v. injection at 300 μg siRAGE/kg and 1.54 mg Dex/kg. There were no significant abnormalities in the representative hematological parameters (white blood cell (WBC); red blood cell (RBC); platelet (PLT); and hemoglobin (HGB)) (Fig. S19 in the ESM). Moreover, negligible changes were found in terms of serum biomarkers, including creatinine (CR), urea (UR), alanine aminotransferase (ALT), and alkaline phosphatase (ALP), indicating minimal systemic toxicity of PPTP@MD/R NCs (Fig. S20 in the ESM).

3 Conclusion

In summary, we rationally engineered the cardiomyocyte-targeted, anti-inflammatory nanotherapeutics for myocardial IR injury based on ROS-ultrasensitive co-delivery of siRAGE and Dex. PPTP enveloping the NCs allowed potent siRNA condensation due to its higher MW, and simultaneously gated the MSNs to prevent the pre-leakage of Dex from the inner cavity. The NCs featured targeted internalization into cardiomyocytes after systemic administration. In the inflamed cardiomyocytes post IR injury, PPTP degraded into small segments in response to the over-produced ROS, releasing the siRAGE and Dex to mediate RAGE down-regulation and provoke cooperative anti-inflammatory outcome. As a consequence, myocardial inflammation, fibrosis, and apoptosis were effectively inhibited, contributing to the restoration of systolic function. Therefore, this study reports an effective example of nanotherapeutics for the co-delivery and on-demand release of nucleic acid and chemodrug payloads, and it might find promising utilities toward the synergistic management of myocardial inflammation.

Acknowledgements

We appreciate the funding support from the National Natural

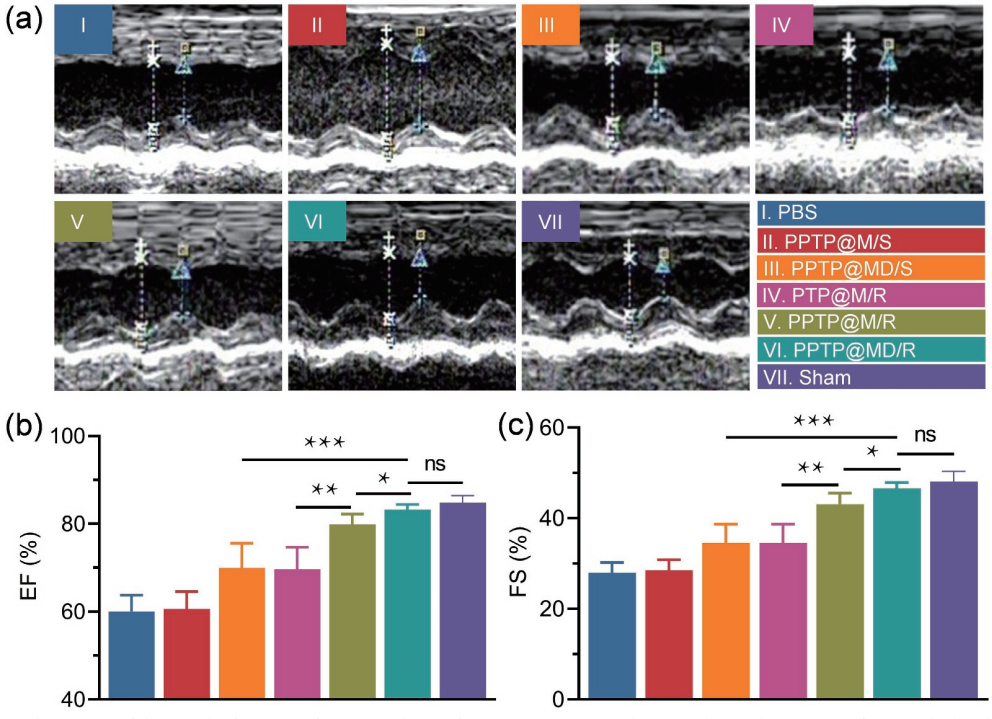

Figure 5 NCs-mediated recovery of the systolic function of IR-injured rats after i.v. injection. (a) Electrocardiographic images of rats. Calculated EF (b) and FS (c) of the left ventricle (n = 4). At 10 min post myocardial IR injury, PBS or NCs were i.v. injected at 1.54 mg Dex/kg and 300 μg siRNA/kg, and electrocardiographic examination was performed at 3 days post injection. Healthy rats without myocardial IR injury were incorporated as the normal control. Differences were assessed to be significant at $^{*}p < 0.05$ and very significant at $^{**}p < 0.01$ and $^{***}p < 0.001$.

Science Foundation of China (No. 52033006 and 51873142), Suzhou Science and Technology Development Project (No. SYS2019072), Collaborative Innovation Center of Suzhou Nano Science & Technology, the 111 project, Suzhou Key Laboratory of Nanotechnology and Biomedicine, and Joint International Research Laboratory of Carbon-Based Functional Materials and Devices.

Electronic Supplementary Material: Supplementary material (experimental methods, RNA and primer sequences, ^{1}H NMR spectra, FTIR spectrum, TEM images, zeta potential, drug loading content, RNA and drug release, cytotoxicity, etc.) is available in the online version of this article at https://doi.org/10.1007/s12274-022-4553-6.

References

[1] Li, Y.; Chen, X.; Jin, R. H.; Chen, L.; Dang, M.; Cao, H.; Dong, Y.; Cai, B. L.; Bai, G.; Gooding, J. et al. Injectable hydrogel with MSNs/microRNA-21-5p delivery enables both immunomodification and enhanced angiogenesis for myocardial infarction therapy in pigs. *Sci. Adv.* **2021**, *7*, eabd6740.

[2] Huang, K.; Ozpinar, E. W.; Su, T.; Tang, J. N.; Shen, D. L.; Qiao, L.; Hu, S. Q.; Li, Z. H.; Liang, H. X.; Mathews, K. et al. An off-the-shelf artificial cardiac patch improves cardiac repair after myocardial infarction in rats and pigs. *Sci. Transl. Med.* **2020**, *12*, eaat9683.

[3] Zhu, D. S.; Li, Z. H.; Huang, K.; Caranasos, T. G.; Rossi, J. S.; Cheng, K. Minimally invasive delivery of therapeutic agents by hydrogel injection into the pericardial cavity for cardiac repair. *Nat. Commun.* **2021**, *12*, 1412.

[4] Li, Z. H.; Hu, S. Q.; Huang, K.; Su, T.; Cores, J.; Cheng, K. Targeted anti-IL-1β platelet microparticles for cardiac detoxing and repair. *Sci. Adv.* **2020**, *6*, eaay0589.

[5] Li, Y.; Chen, X. G.; Li, P.; Xiao, Q. X.; Kong, X. Q. CD47 antibody suppresses isoproterenol-induced cardiac hypertrophy through activation of autophagy. *Am. J. Transl. Res.* **2020**, *12*, 5908–5923.

[6] Li, Z. H.; Zhu, D. S.; Hui, Q.; Bi, J. N.; Yu, B. J.; Huang, Z.; Hu, S. Q.; Wang, Z. Z.; Caranasos, T.; Rossi, J. et al. Injection of ROS-responsive hydrogel loaded with basic fibroblast growth factor into the pericardial cavity for heart repair. *Adv. Funct. Mater.* **2021**, *31*, 2004377.

[7] Hausenloy, D. J.; Yellon, D. M. Ischaemic conditioning and reperfusion injury. *Nat. Rev. Cardiol.* **2016**, *13*, 193–209.

[8] Liu, M. R.; Lutz, H.; Zhu, D. S.; Huang, K.; Li, Z. H.; Dinh, P. U. C.; Gao, J. Q.; Zhang, Y.; Cheng, K. Bispecific antibody inhalation therapy for redirecting stem cells from the lungs to repair heart injury. *Adv. Sci.* **2021**, *8*, 2002127.

[9] Su, T.; Huang, K.; Ma, H.; Liang, H. X.; Dinh, P. U.; Chen, J.; Shen, D. L.; Allen, T. A.; Qiao, L.; Li, Z. H. et al. Platelet-inspired nanocells for targeted heart repair after ischemia/reperfusion injury. *Adv. Funct. Mater.* **2019**, *29*, 1803567.

[10] Liu, C. Y.; Zhang, Y. H.; Li, R. B.; Zhou, L. Y.; An, T.; Zhang, R. C.; Zhai, M.; Huang, Y.; Yan, K. W.; Dong, Y. H. et al. LncRNA CAIF inhibits autophagy and attenuates myocardial infarction by blocking p53-mediated myocardin transcription. *Nat. Commun.* **2018**, *9*, 29.

[11] Tang, Y. Q.; Zeng, Z. Y.; He, X.; Wang, T. T.; Ning, X. H.; Feng, X. L. siRNA crosslinked nanoparticles for the treatment of inflammation-induced liver injury. *Adv. Sci.* **2017**, *4*, 1600228.

[12] Shen, W. W.; Wang, R. J.; Fan, Q. Q.; Gao, X.; Wang, H.; Shen, Y.; Li, Y. W.; Cheng, Y. Y. Natural polyphenol inspired polycatechols for efficient siRNA delivery. *CCS Chem.* **2020**, *2*, 146–157.

[13] Wang, M.; Alberti, K.; Varone, A.; Pouli, D.; Georgakoudi, I.; Xu, Q. B. Enhanced intracellular siRNA delivery using bioreducible lipid-like nanoparticles. *Adv. Healthc. Mater.* **2014**, *3*, 1398–1403.

[14] Yang, J. D.; Duan, S. Z.; Ye, H.; Ge, C. L; Piao, C. X.; Chen, Y. B.; Lee, M.; Yin, L. C. Pro-peptide-reinforced, mucus-penetrating pulmonary siRNA delivery mitigates cytokine storm in pneumonia. *Adv. Funct. Mater.* **2021**, *31*, 2008960.

[15] Hou, M. Y.; Wu, X. J.; Zhao, Z. Y.; Deng, Q. R.; Chen, Y. B.; Yin, L. C. Endothelial cell-targeting, ROS-ultrasensitive drug/siRNA co-delivery nanocomplexes mitigate early-stage neutrophil recruitment for the anti-inflammatory treatment of myocardial ischemia reperfusion injury. *Acta Biomater.* **2022**, *143*, 344–355.

[16] Cai, C. D.; Zhang, X. S.; Li, Y. G.; Liu, X. Z.; Wang, S.; Lu, M. K.; Yan, X.; Deng, L. F.; Liu, S.; Wang, F. et al. Self-healing hydrogel embodied with macrophage-regulation and responsive-gene-

silencing properties for synergistic prevention of peritendinous adhesion. *Adv. Mater.* **2022**, *34*, 2106564.
[17] Shen, S. Y.; Zhang, L.; Li, M. R.; Feng, Z. Z.; Li, H. X.; Xu, X.; Lin, S. Q.; Li, P.; Zhang, C.; Xu, X. J. et al. Collaborative assembly-mediated siRNA delivery for relieving inflammation-induced insulin resistance. *Nano Res.* **2020**, *13*, 2958–2966.
[18] Hong, J.; Ku, S. H.; Lee, M. S.; Jeong, J. H.; Mok, H.; Choi, D.; Kim, S. H. Cardiac RNAi therapy using RAGE siRNA/deoxycholic acid-modified polyethylenimine complexes for myocardial infarction. *Biomaterials* **2014**, *35*, 7562–7573.
[19] Liang, Q. J.; Li, F. F.; Li, Y. J.; Liu, Y.; Lan, M.; Wu, S. H.; Wu, X. J.; Ji, Y.; Zhang, R. J.; Yin, L. C. Self-assisted membrane-penetrating helical polypeptides mediate anti-inflammatory RNAi against myocardial ischemic reperfusion (IR) injury. *Biomater. Sci.* **2019**, *7*, 3717–3728.
[20] Piao, C. X.; Zhuang, C. Y.; Choi, M.; Ha, J.; Lee, M. A RAGE-antagonist peptide potentiates polymeric micelle-mediated intracellular delivery of plasmid DNA for acute lung injury gene therapy. *Nanoscale* **2020**, *12*, 13606–13617.
[21] Dhumal, D.; Lan, W. J.; Ding, L.; Jiang, Y. F.; Lyu, Z.; Laurini, E.; Marson, D.; Tintaru, A.; Dusetti, N.; Giorgio, S. et al. An ionizable supramolecular dendrimer nanosystem for effective siRNA delivery with a favorable safety profile. *Nano Res.* **2021**, *14*, 2247–2254.
[22] Shen, K.; Sun, G. D.; Chan, L.; He, L. Z.; Li, X. W.; Yang, S. X.; Wang, B. C.; Zhang, H.; Huang, J. R.; Chang, M. M. et al. Anti-inflammatory nanotherapeutics by targeting matrix metalloproteinases for immunotherapy of spinal cord injury. *Small* **2021**, *17*, 2102102.
[23] Rinoldi, C.; Zargarian, S. S.; Nakielski, P.; Li, X. R.; Liguori, A.; Petronella, F.; Presutti, D.; Wang, Q. S.; Costantini, M.; De Sio, L. et al. Nanotechnology-assisted RNA delivery: From nucleic acid therapeutics to COVID-19 vaccines. *Small Methods* **2021**, *5*, 2100402.
[24] Nie, J. J.; Qiao, B. K.; Duan, S.; Xu, C.; Chen, B. Y.; Hao, W. J.; Yu, B. R.; Li, Y. L.; Du, J.; Xu, F. J. Unlockable nanocomplexes with self-accelerating nucleic acid release for effective staged gene therapy of cardiovascular diseases. *Adv. Mater.* **2018**, *30*, 1801570.
[25] Hao, K.; Guo, Z. P.; Lin, L.; Sun, P. J.; Li, Y. H.; Tian, H. Y.; Chen, X. S. Covalent organic framework nanoparticles for anti-tumor gene therapy. *Sci. China Chem.* **2021**, *64*, 1235–1241.
[26] Xu, C. F.; Lu, Z. D.; Luo, Y. L.; Liu, Y.; Cao, Z. T.; Shen, S.; Li, H. J.; Liu, J.; Chen, K. G.; Chen, Z. Y. et al. Targeting of NLRP3 inflammasome with gene editing for the amelioration of inflammatory diseases. *Nat. Commun.* **2018**, *9*, 4092.
[27] Weng, Y. H.; Xiao, H. H.; Zhang, J. C.; Liang, X. J.; Huang, Y. Y. RNAi therapeutic and its innovative biotechnological evolution. *Biotechnol. Adv.* **2019**, *37*, 801–825.
[28] Ge, C. L.; Yang, J. D.; Duan, S. Z.; Liu, Y.; Meng, F. H.; Yin, L. C. Fluorinated α-helical polypeptides synchronize mucus permeation and cell penetration toward highly efficient pulmonary siRNA delivery against acute lung injury. *Nano Lett.* **2020**, *20*, 1738–1746.
[29] Hu, B.; Li, B.; Li, K.; Liu, Y. Y.; Li, C. H.; Zheng, L. L.; Zhang, M. J.; Yang, T. R.; Guo, S.; Dong, X. Y. et al. Thermostable ionizable lipid-like nanoparticle (iLAND) for RNAi treatment of hyperlipidemia. *Sci. Adv.* **2022**, *8*, eabm1418.
[30] Wang, C.; Liu, Q.; Zhang, Z. Z.; Wang, Y.; Zheng, Y. D.; Hao, J. L.; Zhao, X. Z.; Liu, Y.; Shi, L. Q. Tumor targeted delivery of siRNA by a nano-scale quaternary polyplex for cancer treatment. *Chem. Eng. J.* **2021**, *425*, 130590.
[31] Ye, L.; Liu, H. M.; Fei, X.; Ma, D.; He, X. Z.; Tang, Q. Y.; Zhao, X.; Zou, H. B.; Chen, X. J.; Kong, X. M. et al. Enhanced endosomal escape of dendrigraft poly-L-lysine polymers for the efficient gene therapy of breast cancer. *Nano Res.* **2022**, *15*, 1135–1144.
[32] Liu, Y.; Yin, L. C. α-Amino acid N-carboxyanhydride (NCA)-derived synthetic polypeptides for nucleic acids delivery. *Adv. Drug Deliv. Rev* **2021**, *171*, 139–163.
[33] Liu, X.; Zhao, Z. Y.; Wu, F.; Chen, Y. B.; Yin, L. C. Tailoring hyperbranched poly(β-amino ester) as a robust and universal platform for cytosolic protein delivery. *Adv. Mater.* **2022**, *34*, 2108116.
[34] Wen, L. J.; Peng, Y.; Wang, K.; Huang, Z. H.; He, S. Y.; Xiong, R. W.; Wu, L. P.; Zhang, F. T.; Hu, F. Q. Regulation of pathological BBB restoration via nanostructured ROS-responsive glycolipid-like copolymer entrapping siVEGF for glioblastoma targeted therapeutics. *Nano Res.* **2022**, *15*, 1455–1465.
[35] Zheng, M.; Liu, Y. Y.; Wang, Y. B.; Zhang, D. Y.; Zou, Y.; Ruan, W. M.; Yin, J. L.; Tao, W.; Park, J. B.; Shi, B. Y. ROS-responsive polymeric siRNA nanomedicine stabilized by triple interactions for the robust glioblastoma combinational RNAi therapy. *Adv. Mater.* **2019**, *31*, 1903277.
[36] Wang, J. X.; He, X. Y.; Shen, S.; Cao, Z. Y.; Yang, X. Z. ROS-sensitive cross-linked polyethylenimine for red-light-activated siRNA therapy. *ACS Appl. Mater. Interfaces* **2019**, *11*, 1855–1863.
[37] Zhang, M. J.; Weng, Y. H.; Cao, Z. Y.; Guo, S.; Hu, B.; Lu, M.; Guo, W. S.; Yang, T. R.; Li, C. H.; Yang, X. Z. et al. ROS-activatable siRNA-engineered polyplex for NIR-triggered synergistic cancer treatment. *ACS Appl. Mater. Interfaces* **2020**, *12*, 32289–32300.
[38] Ye, H.; Zhou, Y.; Liu, X.; Chen, Y. B.; Duan, S. Z.; Zhu, R. Y.; Liu, Y.; Yin, L. C. Recent advances on reactive oxygen species-responsive delivery and diagnosis system. *Biomacromolecules* **2019**, *20*, 2441–2463.
[39] Li, F.; Li, T. Y.; Cao, W.; Wang, L.; Xu, H. P. Near-infrared light stimuli-responsive synergistic therapy nanoplatforms based on the coordination of tellurium-containing block polymer and cisplatin for cancer treatment. *Biomaterials* **2017**, *133*, 208–218.
[40] Zhou, W. Q.; Wang, L.; Li, F.; Zhang, W. N.; Huang, W.; Huo, F. W.; Xu, H. P. Selenium-containing polymer@metal-organic frameworks nanocomposites as an efficient multiresponsive drug delivery system. *Adv. Funct. Mater.* **2017**, *27*, 1605465.
[41] Ji, S. B.; Cao, W.; Yu, Y.; Xu, H. P. Dynamic diselenide bonds: Exchange reaction induced by visible light without catalysis. *Angew. Chem., Int. Ed.* **2014**, *53*, 6781–6785.
[42] Wang, H.; Zhang, S.; Lv, J.; Cheng, Y. Y. Design of polymers for siRNA delivery: Recent progress and challenges. *View* **2021**, *2*, 20200026.
[43] Wen, Y. T.; Bai, H. Z.; Zhu, J. L.; Song, X.; Tang, G. P.; Li, J. A supramolecular platform for controlling and optimizing molecular architectures of siRNA targeted delivery vehicles. *Sci. Adv.* **2020**, *6*, eabc2148.
[44] Zhuang, J.; Gong, H.; Zhou, J. R.; Zhang, Q. Z.; Gao, W. W.; Fang, R. H.; Zhang, L. F. Targeted gene silencing *in vivo* by platelet membrane-coated metal-organic framework nanoparticles. *Sci. Adv.* **2020**, *6*, eaaz6108.
[45] Yan, J.; Liu, X.; Wu, F.; Ge, C. L.; Ye, H.; Chen, X. Y.; Wei, Y. S.; Zhou, R. X.; Duan, S. Z.; Zhu, R. Y. et al. Platelet pharmacytes for the hierarchical amplification of antitumor immunity in response to self-generated immune signals. *Adv. Mater.* **2022**, *34*, 2109517.
[46] Bellis, A.; Mauro, C.; Barbato, E.; Di Gioia, G.; Sorriento, D.; Trimarco, B.; Morisco, C. The rationale of neprilysin inhibition in prevention of myocardial ischemia-reperfusion injury during ST-elevation myocardial infarction. *Cells* **2020**, *9*, 2134.
[47] Hou, M. Y.; Wei, Y. S.; Zhao, Z. Y.; Han, W. Q.; Zhou, R. X.; Zhou, Y.; Zheng, Y. R.; Yin, L. C. Immuno-engineered nanodecoys for the multi-target anti-inflammatory treatment of autoimmune diseases. *Adv. Mater.* **2022**, *34*, 2108817.
[48] Sager, H. B.; Dutta, P.; Dahlman, J. E.; Hulsmans, M.; Courties, G.; Sun, Y.; Heidt, T.; Vinegoni, C.; Borodovsky, A.; Fitzgerald, K. et al. RNAi targeting multiple cell adhesion molecules reduces immune cell recruitment and vascular inflammation after myocardial infarction. *Sci. Transl. Med.* **2016**, *8*, 342ra80.
[49] Wang, Y.; Hou, M. Y.; Duan, S. Z.; Zhao, Z. Y.; Wu, X. J.; Chen, Y. B.; Yin, L. C. Macrophage-targeting gene silencing orchestrates myocardial microenvironment remodeling toward the anti-inflammatory treatment of ischemia-reperfusion (IR) injury. *Bioact. Mater.* **2022**, *17*, 320–333.
[50] Yin, N.; Tan, X. Y.; Liu, H. B.; He, F. M.; Ding, N.; Gou, J. X.; Yin, T.; He, H. B.; Zhang, Y.; Tang, X. A novel indomethacin/methotrexate/MMP-9 siRNA *in situ* hydrogel with dual effects of anti-inflammatory activity and reversal of cartilage disruption for the synergistic treatment of rheumatoid arthritis. *Nanoscale* **2020**, *12*, 8546–8562.
[51] Wang, Q.; Jiang, H.; Li, Y.; Chen, W. F.; Li, H. M.; Peng, K.;

Zhang, Z. R.; Sun, X. Targeting NF-kB signaling with polymeric hybrid micelles that co-deliver siRNA and dexamethasone for arthritis therapy. *Biomaterials* **2017**, *122*, 10–22.

[52] Jiang, K. Y.; Weaver, J. D.; Li, Y. J. Y.; Chen, X. J.; Liang, J. P.; Stabler, C. L. Local release of dexamethasone from macroporous scaffolds accelerates islet transplant engraftment by promotion of anti-inflammatory M2 macrophages. *Biomaterials* **2017**, *114*, 71–81.

[53] Li, X. D.; Wei, Y. S.; Wu, Y. C.; Yin, L. C. Hypoxia-induced pro-protein therapy assisted by a self-catalyzed nanozymogen. *Angew. Chem., Int. Ed.* **2020**, *59*, 22544–22553.

[54] Sun, P. C.; Scharnweber, T.; Wadhwani, P.; Rabe, K. S.; Niemeyer, C. M. DNA-directed assembly of a cell-responsive biohybrid interface for cargo release. *Small Methods* **2021**, *5*, 2001049.

[55] Dong, P.; Hu, J. L.; Yu, S. Y.; Zhou, Y. Z.; Shi, T. H.; Zhao, Y.; Wang, X. Y.; Liu, X. Q. A mitochondrial oxidative stress amplifier to overcome hypoxia resistance for enhanced photodynamic therapy. *Small Methods* **2021**, *5*, 2100581.

[56] Gan, Q.; Zhu, J. Y.; Yuan, Y.; Liu, H. L.; Qian, J. C.; Li, Y. S.; Liu, C. S. A dual-delivery system of pH-responsive chitosan-functionalized mesoporous silica nanoparticles bearing BMP-2 and dexamethasone for enhanced bone regeneration. *J. Mater. Chem. B* **2015**, *3*, 2056–2066.